Composites Science and Technology 256 (2024) 110789

Contents lists available at ScienceDirect

Composites Science and Technology

journal homepage: www.elsevier.com/locate/compscitech

Biomimetic 3D printed spicule-like structure composite of organic material/rigid resin cylinders with highly enhanced strength and toughness

Sorour Sadeghzade [a,b], Niloofar Fani [b], Ajinkya Nene [c], Fariborz Tavangarian [b,d,*]

[a] School of Engineering, Westlake University, Hangzhou, 310024, China
[b] Mechanical Engineering Program, School of Science, Engineering and Technology, Pennsylvania State University, Harrisburg, Middletown, PA, 17057, USA
[c] Laboratory of Inflammation and Vaccines, Shenzhen Institute of Advanced Technology (SIAT), Chinese Academy of Sciences, Shenzhen, 518055, China
[d] Department of Biomedical Engineering, Pennsylvania State University, University Park, State College, PA, 16802, USA

ARTICLE INFO

Handling Editor: Dr. Ming-Qiu Zhang

Keywords:
Spicule
Microstructure
Flexural
Stereolithography
Adhesives

ABSTRACT

Recently, the microstructure of Euplectella Aspergillum (EA) marine sponges, called spicule, has been recognized as one of the attractive biological microstructures with superior flexural strength and toughness. The lack of studies to mimic this structure motivated us to design rods with a spicule-inspired structure with improved mechanical properties. In this study, spicule-inspired structures were produced by the stereolithography (SLA) method. Different adhesives were infiltrated between the layers to evaluate the effect of organic materials on their mechanical properties. The effect of the curing process on the mechanical properties of spicule-inspired structures with and without organic (adhesive) interlayers was evaluated. Also, the effects of various adhesives, different spaces between the cylinders, and ultraviolet (UV) curing on mechanical properties were evaluated. The results showed that the flexural strength of spicule-inspired structures was improved by about 71 % after curing the samples at 60 °C and under UV light for 30 min and aging in the air for 30 days. Samples including Titebond adhesive (SP1-1.1) showed a higher amount of peak load (129.5 ± 17.21 N) and extension (22.3 ± 3.12 mm) compared to those counterparts without any organic layers (SP-1.1) with a peak load of 101.5 ± 13.34 N and extension of 19.1 ± 1.32 mm. Adding the adhesive layers between the rigid cylinders enhanced the flexibility and strength of the structures. It was found that the curing time by UV after 30 days of aging did not affect the mechanical properties of the samples.

1. Introduction

Throughout history, nature has been one of humanity's premier inspirations [1,2]. Recently, the field of biomimetic materials has opened new doors to enhance the quality and properties of materials [3,4]. By studying and mimicking naturally occurring structures, some challenges in architecture, engineering, and material science can be addressed [5,6]. For example, researchers investigated 3D-printed sandwich panels with a trabecular structure core inspired by beetle forewings, focusing on impact performance [7]. Findings showed three distinct stages in force-displacement curves, with perforation of face sheets, core crushing, and final perforation, similar to conventional honeycomb panels [7].

Another example is a nacre-inspired structure as shown in Fig. 1 [8,9]. This structure is a remarkable natural composite material found in the inner shell layer of some mollusks, such as pearl oysters and abalones [10,11]. The hierarchal structure of the nacre is famous for its mechanical strength, toughness, and iridescent appearance [11]. The microstructure of the nacre features thin, flat, hexagonal plates made of aragonite, arranged in a brick-and-mortar pattern as depicted in Fig. 1 [12]. This 3D interlocking structure is supported by an organic matrix of proteins, polysaccharides, and biopolymers, functioning like mortar in the brick-and-mortar analogy [13]. Nacre also displays high elasticity and toughness when exposed to external forces despite the brittleness of its constituent [14,15]. Wang et al. [15] mimicked the structure of Nacre by creating a layered and staggered structural system based on building ceramic mosaic tiles attached to soft adhesive. The results showed that nacre-inspired structures have a high impact resistance and can be used to design and fabricate protective devices [15]. In another study, García et al. [16] explored enhancing fracture toughness in carbon

* Corresponding author. Mechanical Engineering Program, School of Science, Engineering and Technology, Pennsylvania State University, Harrisburg, Middletown, PA 17057, USA.
E-mail addresses: fut16@psu.edu, f.tavangarian@gmail.com (F. Tavangarian).

https://doi.org/10.1016/j.compscitech.2024.110789
Received 5 May 2024; Received in revised form 24 July 2024; Accepted 31 July 2024
Available online 5 August 2024

fiber-reinforced polymer (CFRP) laminates by mimicking nacre's 'brick-and-mortar' structure using automated tape laying (ATL). Mechanisms like crack deflection and resin pockets were identified as enhancing toughness [16].

Also, various studies developed structures derived from hierarchical self-similar structures inspired by snake-like serpentine, bamboo, and honeycomb, varying structure ratios related to cell sizes across different geometric levels [17]. They fabricated these structures via 3D printing to assess energy dissipation through polymer matrices. The bamboo fractal structure with a ratio (β) of 0.2 exhibited the highest energy absorption rates, demonstrating promising potential for engineering applications [17]. In another study [18], the unique hybrid helicoidal microstructure found in the exoskeleton of the American lobster, contrasted it with the previously studied uniform helicoidal structure [18]. Researchers successfully replicated and optimized this hybrid structure using ultra-thin materials in composite laminates. Key findings include enhanced load-bearing capacity and prolonged residual loading rates (PRL), attributes beneficial for applications requiring bends and shear damage resistance, such as protective equipment for athletes or military personnel.

Euplectella Aspergillum (EA) sponges (also known as Venus flower baskets) are another biological structure that received great attention due to their high flexural strength as well as toughness [19,20]. The SEM micrographs and the schematic of the morphological zones of a typical EA sponge were shown in Fig. 1. The skeleton of EA is made of bio-silica and is characterized by a lattice-like structure. The sponge's microstructure exhibits a hierarchical organization with multiple levels of structural complexity called spicules [20,21]. The EA sponge, with a skeleton of at least six hierarchal levels, has varying lengths from centimeters to nanometers and is anchored using thousands of anchor spicules [19,22]. A shield covers each spicule, containing a central proteinaceous axial filament [23,24]. The spicule has an internal structure of a silica core surrounded by axial silica cylinders (cy) and separated by organic layers [24]. These spicules are 5–15 cm in length and between 40 and 70 μm in diameter [25,26]. One of the reasons for the remarkable mechanical properties of EA sponges is the presence of an organic layer called silicatein (Fig. 1) between the hydrate silica cylinders. Crack deflection occurs due to the spicule's cylindrical architecture and the organic interlayers between the brittle amorphous silica cylinders. This helps the sponge withstand high hydrostatic pressures and strong currents in deep-sea environments.

Incorporating layered architectures and hierarchical organization into synthetic materials, similar to natural spicules, helps manage stress and resist fractures by deflecting cracks, dissipating energy, and redistributing loads [27]. Integrating these features into synthetic materials makes achieving enhanced toughness, flexibility, and resistance to catastrophic failure possible. By studying the behavior of EA sponges under flexural and tensile tests, researchers observed a mechanism that can lead to a stress distribution throughout the sponge's brittle structure [28,29]. The concentric cylindrical layers create a flexible microstructure from a brittle material (SiO_2), preventing catastrophic crack propagation [30]. When cracks initiate in one layer, they will be trapped between the cylinders and cannot propagate into the successive layer [31].

Further expansion of cracks into the successive layer requires more force as new cracks should be initiated in the next layer [20]. Therefore, the spicule-inspired structure and the alternating organic/inorganic layers lead to the deflection of the crack path along the cylindrical layers

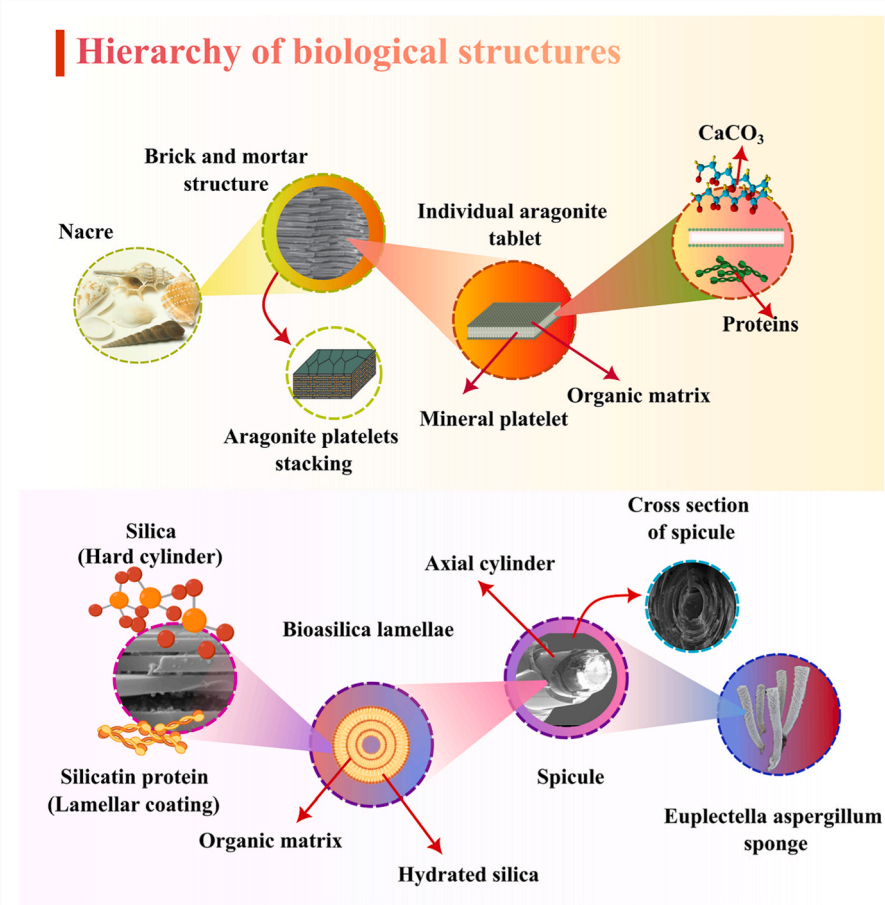

Fig. 1. Hierarchy of biological structures such as nacre and Euplectella Aspergillum (EA), schematic representation, and SEM image of nacre and spicule microstructure and components.

and prevent catastrophic failure [31].

In our previous study [32], we developed rigid resin rods with a spicule-inspired structure (SIS) and compared them with solid rods. Based on the results, the spicule-inspired structure with 0.375 mm cylinder wall thickness without core showed 40.89 ± 5.11 MPa flexural strength and 4.95 ± 0.89 % strain. This sample showed an improvement of 10.5 % in flexural strength and 1450 % in flexural strain compared to the control samples (solid rods). It seems that designing and fabricating nested cylindrical structures (without adhesive interlayers) can partially improve the mechanical properties of brittle synthetic materials. Therefore, to more closely mimic the structure of spicules, in the present study, we developed nested cylindrical structures with organic adhesive interlayers (different types of glues) to evaluate the effect of organic interlayers on the mechanical behavior of SISs. Different glues and various interlayer spacing were considered to investigate their effects on the mechanical properties of SISs composites. These lightweight nested

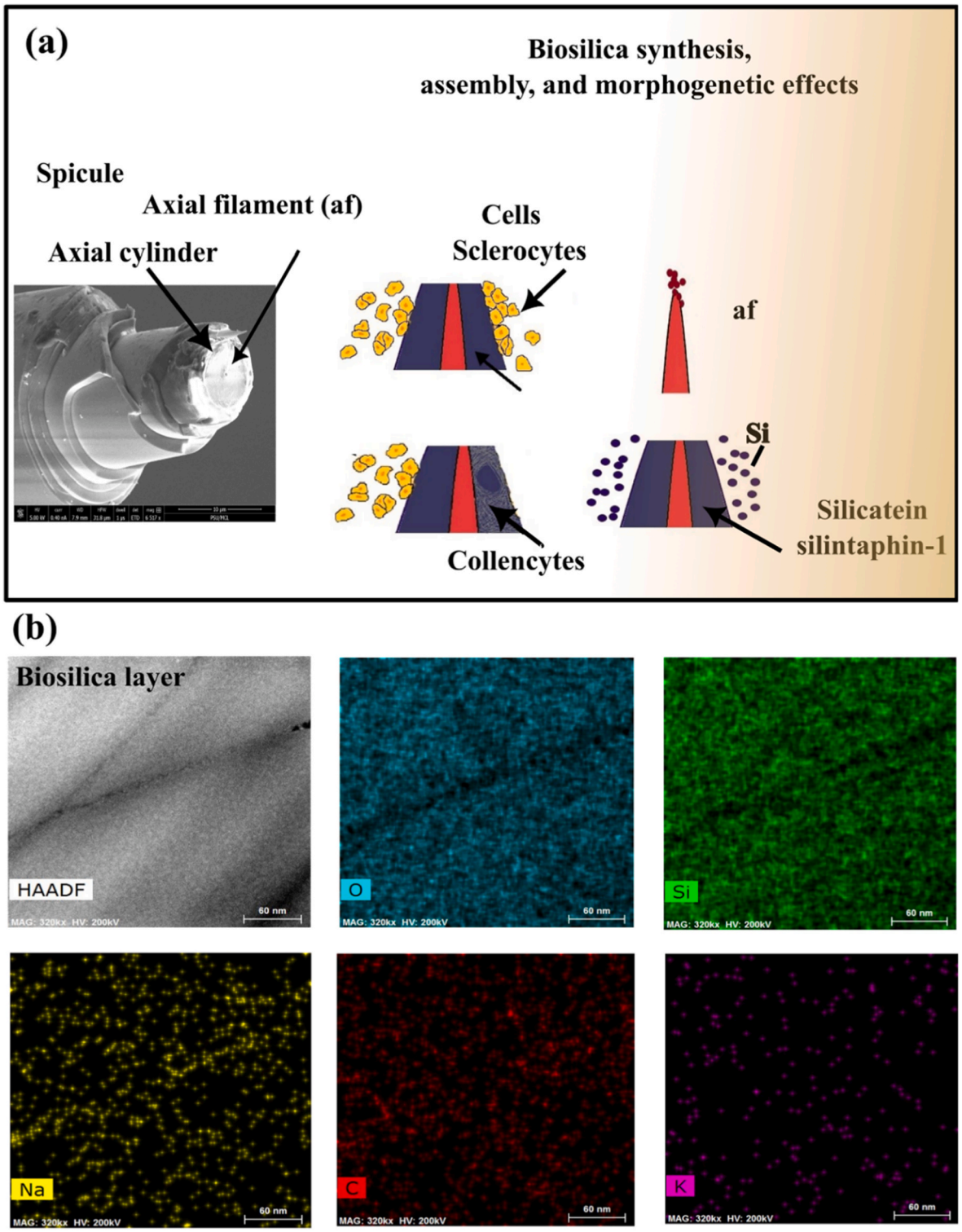

Fig. 2. (a) natural spicule composition and schematic representation of bio-silica synthesis, assembly and morphogenetic effects, (b) HAADF-STEM images and EDS mapping of natural spicule.

cylindrical structures with enhanced mechanical properties and flexibility showed a crack deflection mechanism during the 3-point bending test. They can change the mode of fracture from catastrophic failure to gradual one.

2. Materials and methods

2.1. Mimicking spicule microstructure

To replicate the spicule microstructure, it's crucial to analyze its biological architecture, focusing on the cellular processes behind silica biosynthesis and assembly. We utilized High-angle Annular Dark-Field Imaging with transmission electron microscopy (HAADF-STEM, ThermoFisher Scientific, Talos F200c, USA) to investigate the microstructure of natural spicules at a nanoscale level. This technique offers high-resolution imaging capabilities, allowing us to examine the intricate details of the spicule's internal structure, including the arrangement of nanoparticles and the distribution of organic and inorganic components.

Fig. 2a shows that spicule formation starts with an axial filament, surrounded by splenocytes involved in biosilica deposition. Enzymatic proteins like silicatein and silintaphin-1 play key roles, highlighting the organic-inorganic interface where biomineralization occurs [22].

Also, the HAADF-STEM images and elemental mapping of bio-silica layers are shown in Fig. 2b. The image (Fig. 2b) allows visualization of the two spicules' cylinder structure. The subsequent images are elemental maps showing the distribution of specific elements within the biosilica layer: oxygen (O), silicon (Si), sodium (Na), carbon (C), and potassium (K). These EDS maps are used with STEM microscopy to identify and quantify the elemental composition of the spicule layer. The distribution of elements reveals the inorganic (Si, O) and organic (C, potentially from organic matrices) components, as well as other elements like Na and K that might be involved in the biological processes of biosilica formation or are present in the ambient marine environment where these organisms exist. This detailed imaging and analysis help us understand the intricate process of biomineralization, which is crucial for developing biomimetic materials and structures.

2.2. Materials

The rigid resin (RR, FLRGWHO1) was purchased from Formlabs® company in the USA [33]. We selected this resin type because it is reinforced with glass particles (SiO_2), providing high stiffness and a polished finish. This material is particularly resistant to deformation over time and is well-suited for printing thin walls and intricate features. It exhibits brittle behavior and offers a flexural modulus of 3.7 GPa and a tensile modulus of 4.1 GPa, demonstrating excellent heat resistance and stability. Isopropyl alcohol (IPA, 91 %) was received from Florida Laboratories, Inc. A RR printed sample with immersed in isopropyl alcohol (IPA) for 24 h was shown a very low percent weight gain (about 0.4 %) [33]. This indicates that IPA has minimal absorption into the printed material, suggesting it is effective for washing printed samples without causing significant swelling or deformation. Several types of glue (soft and rigid) were utilized, including E6000 (230010 Industrial Strength Adhesive), Loctite Superglue (Superglue, Henkel Corporation, Ireland), Starbond (KBL-500 Glue, Japan), Titebond (5013 Liquid Hide Glue, Franklin International, Ohio), and Old Brown glue (Old Brown, Antique Refinishers INC. USA).

2.3. Fabrication procedure of SIS

In order to prepare the rods with SISs, the stereolithography (SLA) technique was used, and rigid resin (RR, FLRGWHO1) was used as the initial material. 3D models of SISs with 0.375 mm wall thickness with five layers (printed at the same time as shown in Figs. 3) and 170 mm height were designed by SolidWorks [32]. Then, the STL files of CAD models were uploaded to Preform software (*Formlabs*® company, USA), which prepares the models to be printed. In order to achieve the highest resolution and quality of the printed samples, the thickness of each slice was adjusted to 50 μm. The CAD model was sliced into 3396 layers based on the model height (170 mm) and the thickness of each slice.

Fig. 3 shows a schematic representation of the *Form 2* printer used in this study. As can be seen, the samples were printed simultaneously by *Form 2* 3D printer with a laser spot size of 140 μm, laser thickness of 25 μm, and laser power of 250 mW.

The dimensions of samples were chosen according to ASTM D790-15 for the 3-point bending test and the maximum length of samples that could be 3D printed by *Form 2* [34]. The space between the concentric cylindrical layers was selected as 1.1-, 1.2-, 1.3-, 1.4-, and 1.5-mm. Table 1 demonstrates the designation and specification of all samples. The automated *Form Wash* (*Formlabs*® company, USA) with isopropanol alcohol (IPA, 99 %) was used to wash all samples after printing.

2.4. Fabrication procedure of SIS composites

The composite samples, designed to replicate a spicule-inspired structure with organic and rigid resin components, were manufactured using a vacuum pump to suck organic materials between the RR cylinders (Fig. 3). To facilitate the infiltration of glues between the cylindrical layers, a hose was connected to the end of the SISs (Fig. 3), with the other end linked to the vacuum pump. Each SIS was immersed in glue, and upon activating the pump, the glue was drawn into the space between the layers. Accurate measurement of the layer spacing ensured the precise application of glue, which is crucial for maintaining structural integrity. Vacuum assistance ensured the even distribution of the glue throughout the interlayer space. After the infusion, samples were put in an environment for one month to dry. The organic materials used included various types of glue: E6000, Superglue, Starbond, Titebond, and Old Brown. These organic materials were chosen deliberately for their distinct mechanical properties, some being brittle and others very ductile. This selection aimed to investigate how different types of organic layers influence the mechanical properties of the composite when combined with the rigid resin. The goal was to observe and analyze how the brittleness or ductility of these organic materials affects aspects such as strength, toughness, and resilience of the final composite

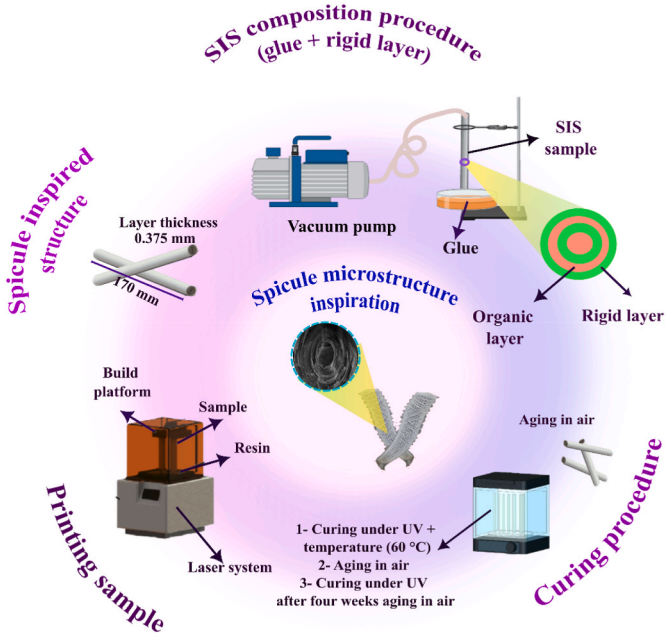

Fig. 3. Schematic representation of fabrication procedure of spicule-inspired structure (SISs) with 3D-printing method including adhesive interlayers and curing procedure of different samples.

Table 1
Designation and three curing procedures of different specimens.

			Curing procedures		
			First step	Second step	Third step
samples	Space between layers (mm)	Type of glue	Curing under UV + temperature (60 °C)	Aging in air for four weeks for simple and composite samples	Curing under UV after four weeks aging in air
SP-1.1-N (sample without any curing procedure)	1.1	–	–	–	–
SP-1.1	1.1	–	✓	✓	×
SP-1.2	1.2	–	✓	✓	×
SP-1.3	1.3	–	✓	✓	×
SP-1.4	1.4	–	✓	✓	×
SP-1.5	1.5	–	✓	✓	×
SP1-1.1	1.1	Titebond	✓	✓	×
SP1-1.2	1.2	Titebond	✓	✓	×
SP1-1.3	1.3	Titebond	✓	✓	×
SP1-1.4	1.4	Titebond	✓	✓	×
SP1-1.5	1.5	Titebond	✓	✓	×
SP2-1.1	1.1	Starbond	✓	✓	×
SP3-1.1	1.1	E6000	✓	✓	×
SP4-1.1	1.1	Superglue	✓	✓	×
SP5-1.1	1.1	Old brown	✓	✓	×
SPU-1.1	1.1	–	✓	✓	✓
SP1U-1.1	1.1	Titebond	✓	✓	✓
SP2U-1.1	1.1	Starbond	✓	✓	✓
SP3U-1.1	1.1	E6000	✓	✓	✓
SP4U-1.1	1.1	Superglue	✓	✓	✓
SP5U-1.1	1.1	Old brown	✓	✓	✓

structure.

2.5. Curing procedure of samples

In this study, we performed three processes to cure simple and composite samples. In the first step, all printed samples were cured at *Form Cure* (*Formlabs*® company, FH-CU-01, USA) under 60 °C for 30 min and 13 multi-directional LED lights with an ultraviolet light wavelength of 405 nm, LED power of 39 W, and LED radiant of 9.1 W.

In the second step, the SIS composites (including glue between the cylindrical layers) were completely cured at the environment temperature for four weeks. In the third step, some samples were cured in *Form Cure* under UV for 30 min at room temperature.

2.6. Fourier transform infrared spectroscopy test

In order to determine the functional groups of rigid resin before and after the curing process, the Fourier transform infrared spectroscopy (FTIR, JASCO 680 PLUS) was used in the range of 370–4000 cm^{-1}.

2.7. Microscopic analysis

In order to determine the crack propagation patterns and toughening mechanism of different samples at a macroscopic and microscopic scale, optical microscopy technique (Smartzoom5, Digital microscope, Carl-Zeissss-Promenade 10, Germany) and scanning electron microscopy (SEM) coupled with energy-dispersive spectroscope (EDS) (Thermo-scientific, Apreo S) were carried out.

2.8. Density measurement

The density of samples was measured by DahoMeter DE-120 M densimeter to normalize the mechanical properties of the samples based on their density.

2.9. 3-Point bending test

Different samples' flexural strength (3-point bending test) was tested using a universal testing machine (MTS Insight, Electromechanical 30 kN Standard Length). The crosshead speed and the span were adjusted to 20 mm/min and 160 mm, respectively. For each test, five specimens were evaluated. The flexural strength, strain, and modules of the SISs with circular cross-sections were calculated according to Ref. [34]. The flexural stress, strain, and modules were calculated according to equations (1)–(3), respectively [35]:

$$\sigma = \frac{MC}{I} \tag{1}$$

Where M is the bending moment, C is distance from the neutral axis (mm) and I is the moment of inertia (for cylinders, $I_{cy} = \frac{\pi}{64\left(d_2^4 - d_1^4\right)}$, and for core, $I_c = \frac{\pi}{64d^4}$). The strain can be calculated as follow:

$$\varepsilon = \frac{6Dd}{L^2} \tag{2}$$

Where D is the maximum deflection of the center of the beam (mm) and d is depth or thickness of the sample (mm). The elastic modulus can be calculated as:

$$E = \frac{L^3 m}{12\pi R^4} \tag{3}$$

Where m is the gradient (slope) of the initial straight-line portion of the load displacement curve [36]. Furthermore, the absorbed energy was calculated from the area under the force-displacement curves.

2.10. Statistical analysis

Each experiment's data were expressed as mean ± standard deviation (SD). Statistical analysis was performed using one-way ANOVA and Tukey's test. Differences were measured as statistically significant at $P<0.05$.

3. Results and discussion

3.1. Rigid resin characterization

The FTIR results of rigid resin before and after the crosslinking process (after printing, curing with *Form cure*, and aging in the air) were

shown in Fig. 4a–d and Table S1 in the supplementary materials. The FTIR spectra of the liquid rigid resin (Fig. 4a) exhibited characteristic absorption peaks for C–H (2880–2950 cm^{-1} and 1300–1360 cm^{-1}), O–H (850–950 cm^{-1} and 3200–3300 cm^{-1}), CH_2 (1531, 1440–1480, and 1370–1390 cm^{-1}), and C═O and C═C (1720 cm^{-1} and 1637 cm^{-1} respectively). Peaks for C–O were detected at 1230–1260 cm^{-1}, 1165–1185 cm^{-1}, and 1050–1100 cm^{-1}, while Si–*O*–Si peaks appeared in the range of 940–1050 cm^{-1} and 650–780 cm^{-1}, with Si–OH around 813 cm^{-1}.

Upon printing (Fig. 4b), reduced peak intensities and shifts in C═C (1635 cm^{-1}) and C═O (1709 cm^{-1}) were noted. Further curing with Form cure (Fig. 4c) resulted in the disappearance of C–H peaks and a reduction in CH_2 peak intensity. Shifts and reductions in Si–*O*–Si peaks, along with increased Si–OH intensity at 793 cm^{-1}, were observed. After 30 days of aging (Fig. 4d), C═O and C═C peaks disappeared entirely, indicating complete crosslinking.

The FTIR patterns confirmed the presence of vinyl, carboxyl, hydroxyl, and ester groups, indicating acrylate and methacrylic-based polymers, alongside SiO_2 glass particles. Evaluating the composition and reactions during printing is crucial as it reveals how these interactions enhance the mechanical properties of the spicule-inspired structure (SIS). The complete crosslinking observed over time suggests that the interaction between the resin and SiO_2 particles significantly improves the structural integrity and mechanical strength of the SISs [37–45].

Fig. 4e–g presents the schematic representation of the curing process for rigid resin, which comprises methacrylic monomer, photoinitiator, and SiO_2 glass particles. FTIR results (Fig. 4e) showed the initial molecular structure of the resin. After curing (Fig. 4f), UV light absorbed by photoinitiators generated free radicals, breaking C═C and C═O bonds. The resulting highly reactive free radicals continued reacting until monomer depletion (Fig. 4g). These findings align with the FTIR results (Fig. 4a–d). Additionally, hydroxyl groups (OH) are crucial for bonding resin to silica particles, forming Si–OH groups that chemically react with C–O• and C–C• radicals in the resin, enhancing the bond strength. The SEM and EDS analyses of SP-1.1 (Fig. 4h and i) confirmed the presence of SiO_2 particles, with Ir peaks from the coating process. This crosslinking and interaction between glass particles and resin are key to improving the mechanical properties of SISs.

The microstructure of an SP-1.1 cylinder (Fig. 4j) shows spherical rigid resin grains with an average particle size of 0.716 ± 0.05 μm, forming a uniform, pore-free structure. SEM images of natural spicule structures (Fig. 4k) reveal silica cylinders made of small colloids (50–200 nm), with SAXS results indicating even smaller colloids (2.8 nm) in natural spicules. The similarity in particle morphology between SISs and natural spicules suggests that SISs can activate similar strengthening mechanisms [24].

3.2. Flexural behavior of SIS sample

The load and displacement of various SISs at peak load and load at failure point were shown in Fig. 5. The flexural strength, flexural strain and modulus of SISs with various types of glues were compared with those obtained from SISs without any organic interlayers and have shown in Fig. 6. As can be seen in Fig. 5, SP-1.1 (without any glues) showed the peak load, and load at final fracture point and displacement at these two points of 101.5 ± 13.34 N, 51 ± 10.23 N, 19.1 ± 1.32 mm and 53.2 ± 3.45 mm, respectively. Meanwhile, various types of glue

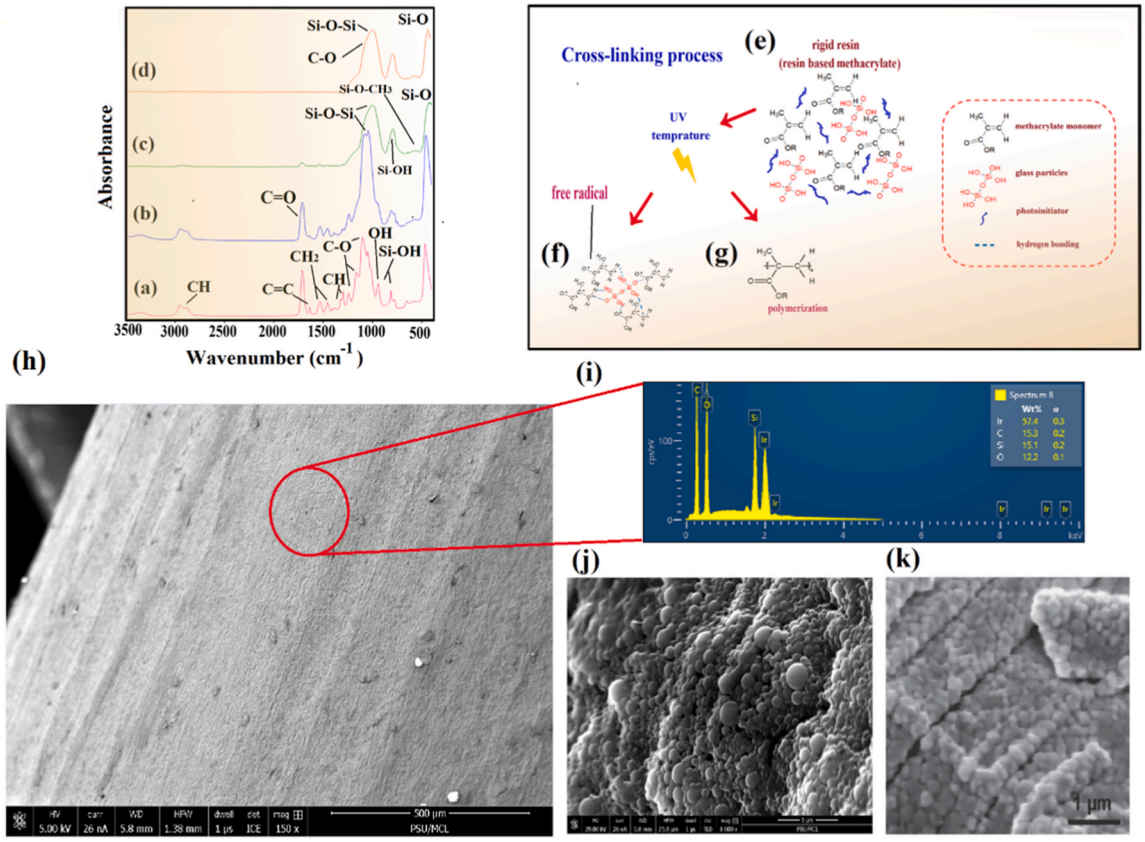

Fig. 4. The FTIR spectrum of (a) liquid rigid resin, (b) cured rigid resin with *Form 2* printer, (c) after curing with *Form cure*, (d) cured after aging for 30 days in air, (e–g) cross-linking process of rigid resin, (h) SEM micrograph of 3D printed rigid resin cylinders, (i) EDS spectra of a printed rigid cylinders (Ir peaks is related to conductive coating on the sample), (j) The SEM micrograph of the 3D printed rigid resin cylinders, shown at higher magnification, reveals a microstructure that closely resembles that of natural spicules (K) [24]. This similarity underscores the appropriateness of the crosslinking process and the selection of materials, confirming their effectiveness in achieving the desired structural properties.

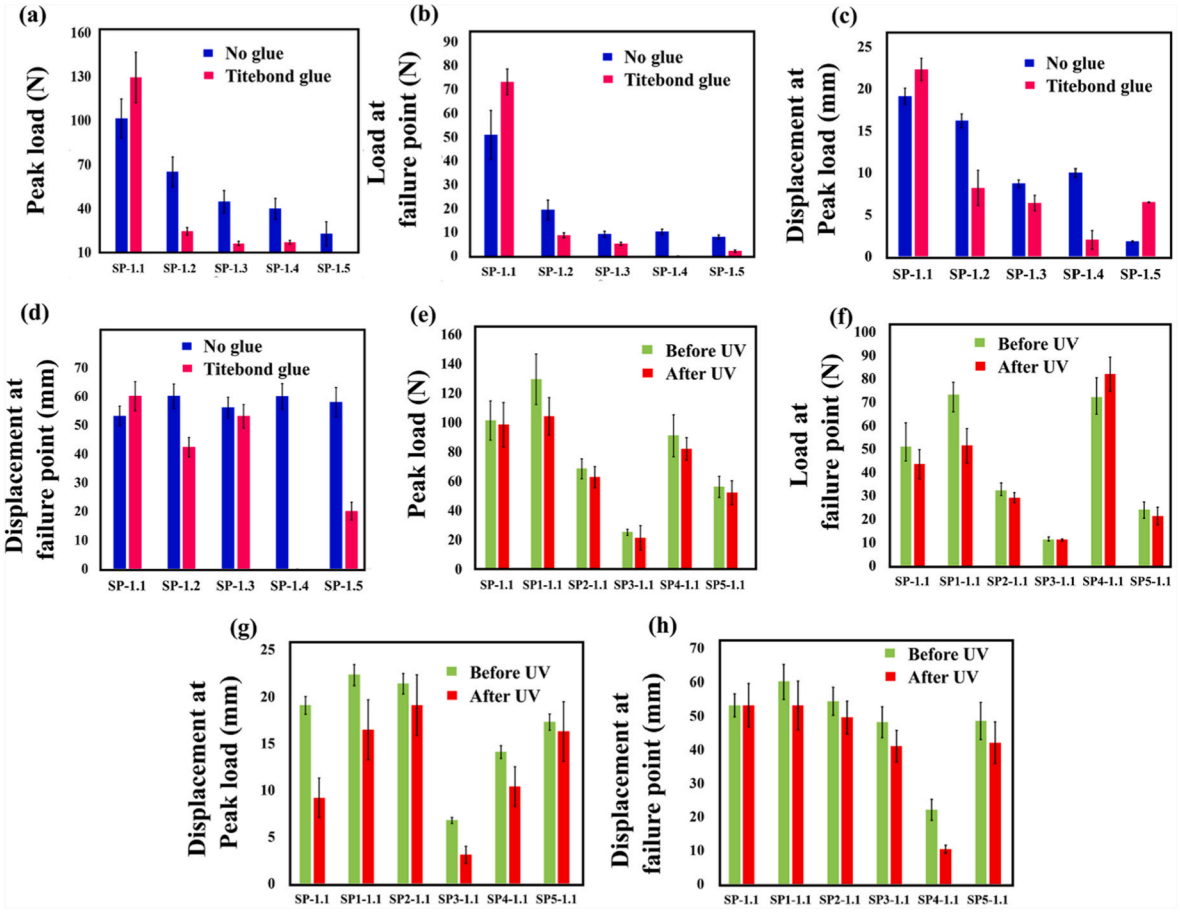

Fig. 5. The load and displacement of various SISs at peak load and load at the failure point are presented in graphs (a–d), comparing samples with and without Titebond glue for different spacing between the layers, and (e–h) the load and displacement for samples with a 1.1 mm spacing between layers, both before and after UV curing with different types of glue.

between the rigid resin cylinders caused different behaviors under flexural test. Among all the samples, SP1-1.1 (including Titebond glue between the cylindrical layers) with peak load and displacement of 129.5 ± 17.21 N and 22.3 ± 3.12 mm showed the highest flexural force (Fig. 5).

Also, the load and displacement at the fracture point increased from 51 ± 10.23 MPa and 53.2 ± 3.45 mm (for SP-1.1 sample) to 73.2 ± 5.34 mm and 60.1 ± 5.1 (for SP1-1.1), respectively. The schematic representation of composite SISs before and during the 3-point bending test was shown in Fig. 6a. As can be seen, the SISs, including organic interlayers, demonstrated a robust structure with significant flexibility. In these samples, a very small crack is initiated at the surface of the rigid layer, and as a result of the applied force, the crack is propagated throughout the thickness of the cylinders. As the crack reaches the adhesive layer, a large amount of crack energy is absorbed by this layer, making it difficult to propagate further. Adhesive layers can dissipate energy through various mechanisms, such as plastic deformation or viscoelastic processes [46].

Fig. 6b demonstrates the typical flexural load extension of different samples. As can be seen, SP-1.1 showed a load-extension curve similar to that of SP1-1.1, SP2-1.1, SP3-1.1, and SP5-1.1. At the same time, the load-extension curve of SP4-1.1 exhibited a different load-extension curve and, subsequently, different mechanical properties. In all samples except SP4-1.1, the elastic and plastic regions can be seen. Those samples showed ductile behavior. However, they were made from brittle materials. As can be seen in Fig. 6c–e, among all adhesives that have been used in this study, the SIS composites, including Titebond (SP1-1.1), showed the best mechanical properties (maximum flexural strength ~ 51.95 ± 6.53 MPa, 28 % improvement compared to SP-1.1 with maximum flexural strength ~ 40.72 ± 4.31 MPa and solid sample with 39 ± 4.51 MPa flexural strength).

Adding adhesives such as Starbond, Old brown, E6000, and Superglue reduced the maximum flexural strength to 27.49 ± 3.21 MPa, 22.56 ± 2.56 MPa, 10.12 ± 1.56 MPa and 36.51 ± 3.54 MPa, respectively. The adhesives used in this study (Starbond, Titebond, Old Brown, E6000, and Superglue) exhibit varying viscosities, shrinkage, and adherence properties, significantly affecting their ability to fill spaces and bond layers effectively. Adhesives with high viscosity, such as E6000 and Old Brown, cannot to fully penetrate gaps (even by applying vacuum), while those with very low viscosity, like Starbond and Superglue, result in insufficient filling and bonding. Additionally, variations in surface tension and the adhesive's wettability on rigid resin can impede the adhesive's ability to spread and fill voids. The degree of shrinkage upon drying also impacts the effectiveness of adhesives in filling spaces; high shrinkage can create voids and reduce contact areas, thereby compromising the mechanical properties of the bonded structure. This shrinkage is particularly problematic for adhesives with low initial viscosity, as they tend to recede more during curing. Moreover, the method of adhesive application including factors such as pressure, temperature, and application speed affects the degree of filling. Differences in these parameters during experiments could have contributed to incomplete filling.

As shown in Fig. 7a, the adhesives in SP2-1.1, SP3-1.1, SP4-1.1 and SP5-1.1 could not fill the space between the cylinders and adhere the rigid layers together. In SP1-1.1, the Titebond glue filled the space between the layers, which is the main reason for improved flexural

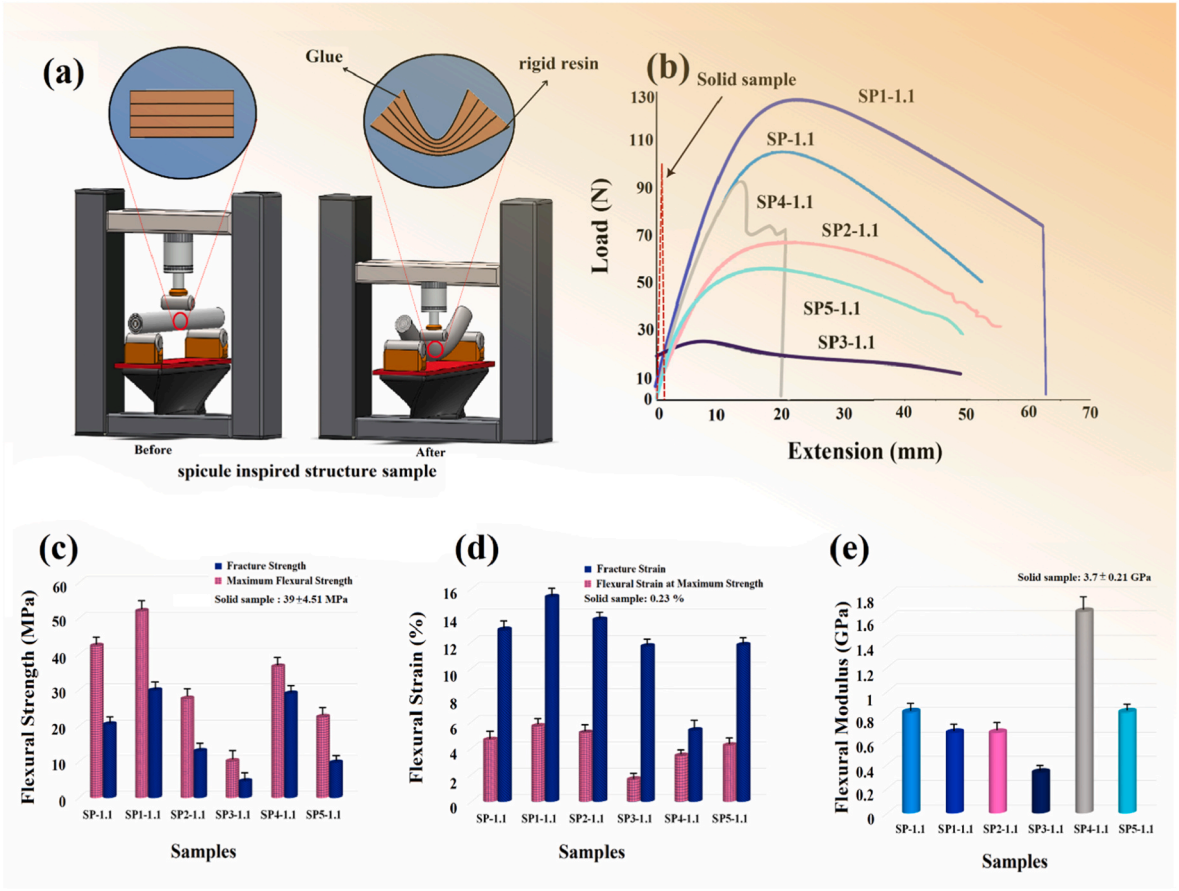

Fig. 6. (a) Schematic representation of SP1-1.1 before and during the 3-point bending test, (b) corresponding load-extension curves, comparison of flexural (c) strength, (d) strain and (e) modulus of SISs samples with and without various glues.

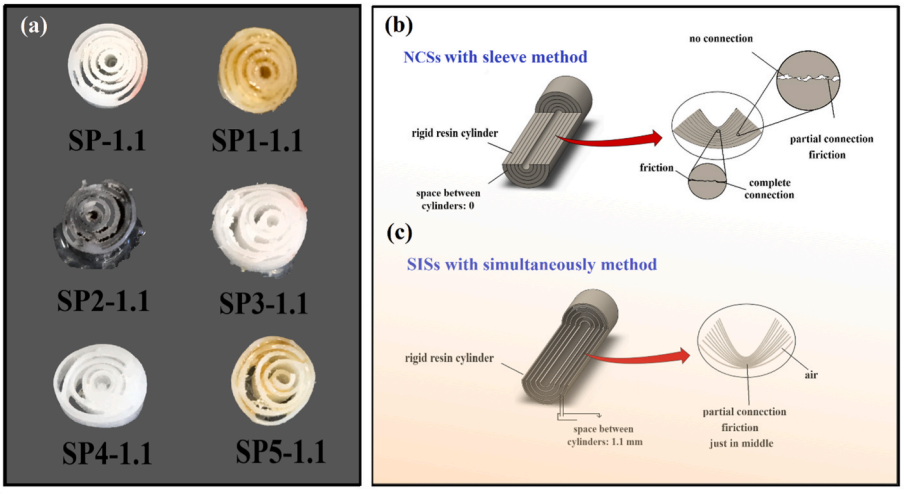

Fig. 7. (a) SISs samples cross-sections with various glues, (b–c) contrasting mechanical behaviors of nested cylindrical structures: a comparative analysis of sleeve versus simultaneous fabrication methods.

strength, strain, and modulus compared to other samples.

Fig. 6d exhibited the flexural and fracture strain of various specimens. Compared to SP-1.1 with flexural and fracture strain of 4.62 ± 0.78 % and 12.87 ± 1.34 %, respectively, among all the SISs, SP1-1.1 showed the highest flexural strain (5.39 ± 1.11 %) and fracture strain (14.54 ± 1.42 %). The results showed that the elastic modulus of all composite samples, except the SP4-1.1, reduced compared to SP-1.1. The elastic modulus demonstrates the stiffness of a material; hence, the presence of soft or tough phases can affect it. For example, the dried Superglue between the layers created a brittle phase and subsequently caused an increase in the elastic modulus and stiffness. In contrast, other glues generated soft phases, which consequently decreased the stiffness of the SISs (the viscous-plastic behavior can be observed in those samples).

After four week aging period, treating the samples with UV light for 30 min resulted in a reduction in the bending strength as follows: SPU-1.1 by 3 %, SP1U-1.1 by 20 %, SP2U-1.1 by 8 %, SP3U-1.1 by 15 %, SP4U-1.1 by 9 %, and SP5U-1.1 by 7 %. Based on the results, it became evident that it did not effectively enhance the mechanical properties of spicule-inspired structures. Therefore, it is not recommended to pursue this approach to improve long-term application reliability across various fields.

3.3. Factors influencing the mechanical behavior of SIS sample

The observed behavior in SIS samples can be attributed to several factors. Firstly, the bioinspired spicule structures with concentric cylindrical layers effectively prevent catastrophic failure of the specimens. Implementing the spicule architecture in solid rods prevents the propagation of cracks through the whole structure and consequently prevents catastrophic failure. The cylinders can act as a barrier for the propagation of the cracks during the mechanical test. Meanwhile, solid rods made with rigid resin failed catastrophically, and only the elastic region could be observed in their load-extension curves. The second reason for such behavior can be the space between the concentric cylinders in the SISs. SISs with 1.1 mm space between the cylindrical layers showed a higher flexibility. In this case, there is enough space between the cylindrical layers to slide over each other easily. In our previous [47] study, nested cylindrical structures (NCSs), which draw design inspiration from the robustness of spicules, were engineered using a precise sleeve fabrication technique. In this approach, the cylindrical layers were configured in the design phase to ensure a zero-tolerance fit, as reflected in the CAD models where no space was allocated between adjacent layers. When subjected to flexural testing, the closely fitted layers of these sleeve-method NCSs encountered resistance to sliding against each other due to the designed absence of interlayer space. This design led to a characteristic step-wise fracture under stress, indicative of a controlled and phased failure mechanism. The layers' direct and multiple contact points along the length of the specimens resulted in significant frictional forces. This friction further engaged an interlocking effect, preventing the layers from moving freely and contributing to the observed gradual failure process.

SISs fabricated using a simultaneous method, where a deliberate 1.1 mm gap was maintained between layers, presented a contrasting mechanical response. In these structures, as demonstrated in Fig. 7c, layer contact and friction are limited to the central region directly under the applied load during bending. The minimized friction means this configuration does not activate the interlocking mechanism intrinsic to the sleeve method structures. Consequently, the simultaneous method NCSs exhibit a notable increase in flexibility but a decrease in structural strength. This comparison between these two methods underscores a key insight: the design and fabrication approach significantly influence the mechanical behavior of the NCSs. Structures built with the sleeve method prioritize strength and structural integrity through enhanced friction and interlocking, while those produced by the simultaneous method favor flexibility due to reduced interlayer friction. Such findings are essential for tailoring the mechanical properties of NCSs for specific applications where the balance between strength and flexibility is crucial.

The third factor is due to the presence of adhesive layers between the concentric rigid cylinders. The presence of adhesive layers between the rigid layers is similar to the silicatein (organic layer) between the hydrate silica concentric cylinders [29]. The presence of organic layers (silicatein) between the concentric silica cylinders in spicules leads to energy dissipation, energy absorption, discontinuation of crack propagation, and crack deflection [31]. Therefore, we expected that adding the adhesive layers to SISs would generate similar results.

In the 3-point bending test, normal and shear stresses were exerted on the samples, causing their failure. In analyzing fracture mechanics within structures inspired by spicules, the simultaneous fabrication method reveals unique behavior under bending stress. This method places thin-walled cylinders in proximity without adhesive, differing significantly from sleeve methods. The thinness of the cylinders and the gaps (as in SP-1.1) serve as critical barriers to crack initiation and propagation. In SP1-1.1, where the adhesive is present, the adhesive layer moderates the interaction between the rigid cylinders, thus altering the stress distribution and hindering direct crack progression.

3.4. Analysis of crack propagation and toughening mechanisms in SIS sample

Optical microscopy (OM) images (Fig. 8) demonstrate that in SP1-1.1 and SP-1.1, cracks tend to develop longitudinally along the tension zone on the underside of the structure. However, due to the limited force exerted along the length of the cylinders and their minimal thickness, there is a significant reduction in stress transmission from the interior to the exterior. As a result, cracks are challenging to develop in this direction. Microscopically, as the main crack attempts to extend, irregularities at the grain level may interlock across the crack faces, necessitating additional energy for fracture completion. This interruption in crack progression leads to new, energetically favorable cracks elsewhere as the applied bending force persists, and the structure must dissipate this energy.

Macroscopically, crack bridging is also evident in the structure, where the adhesive layer's flexibility and the rigidity of the cylinders interplay to impede the cylinders' separation. This interaction also captures the energy from the bending force, dampening the propagation of a single, catastrophic fracture. Crack bifurcation, another observed toughening mechanism, is favored as it occurs at lower energy thresholds, thereby absorbing energy and preventing rapid, brittle failure.

Quantitative assessment in Fig. 5 reveals that an increase in interlayer space filled with Titebond glue leads to a decrease in peak load, implying that excessive adhesive thickness weakens the structure. This is likely because thicker adhesive layers require extended curing times, potentially leaving the adhesive incompletely set and compromising structural integrity. Conversely, the rigid cylinders predominantly contribute to structural strength, while the adhesive layers enhance flexibility.

The SEM micrographs of the fracture surfaces of a sample without any glue (SP-1.1) and samples with Titebond (SP1-1.1) and Superglue (SP4-1.1) and the schematic representation of the toughening mechanism of the SISs are shown in Fig. 9. These images show the fracture morphology and crack propagation paths, with annotations highlighting significant features such as river lines, changes in fracture direction, and glue interfaces.

Fig. 9a–c illustrates the cleavage facets in each cylinder resulting from the interaction between glass particles and crack propagation in the matrix (river-like patterns). This is an indication of the brittle fracture in each layer. One of the key toughening mechanisms in SISs is crack deflection (Fig. 9j). In SISs, crack initiation and propagation do not occur in a single plane but are randomly dispersed throughout the structure. The spaces between successive layers act as barriers to crack propagation from the outer surface toward the center. These empty spaces resist crack propagation and consequently absorb energy, as generating new cracks in the next layers requires higher energy. The empty spaces between successive layers are perpendicular to the crack propagation direction induced by the applied external force during the 3-point bending test. Thus, they can act as barriers and stop crack growth. Similar mechanisms have been reported in natural spicules [32].

In addition, applying glue between the layers can activate another toughening mechanism, as seen in Fig. 9d–i, the toughening and strengthening mechanisms in SISs significantly influence the glue used to bond the cylinders. When ductile glue is used (SP1-1.1), it can enhance energy dissipation and contribute to toughening by allowing plastic deformation at the glue interfaces. This ductile behavior helps to

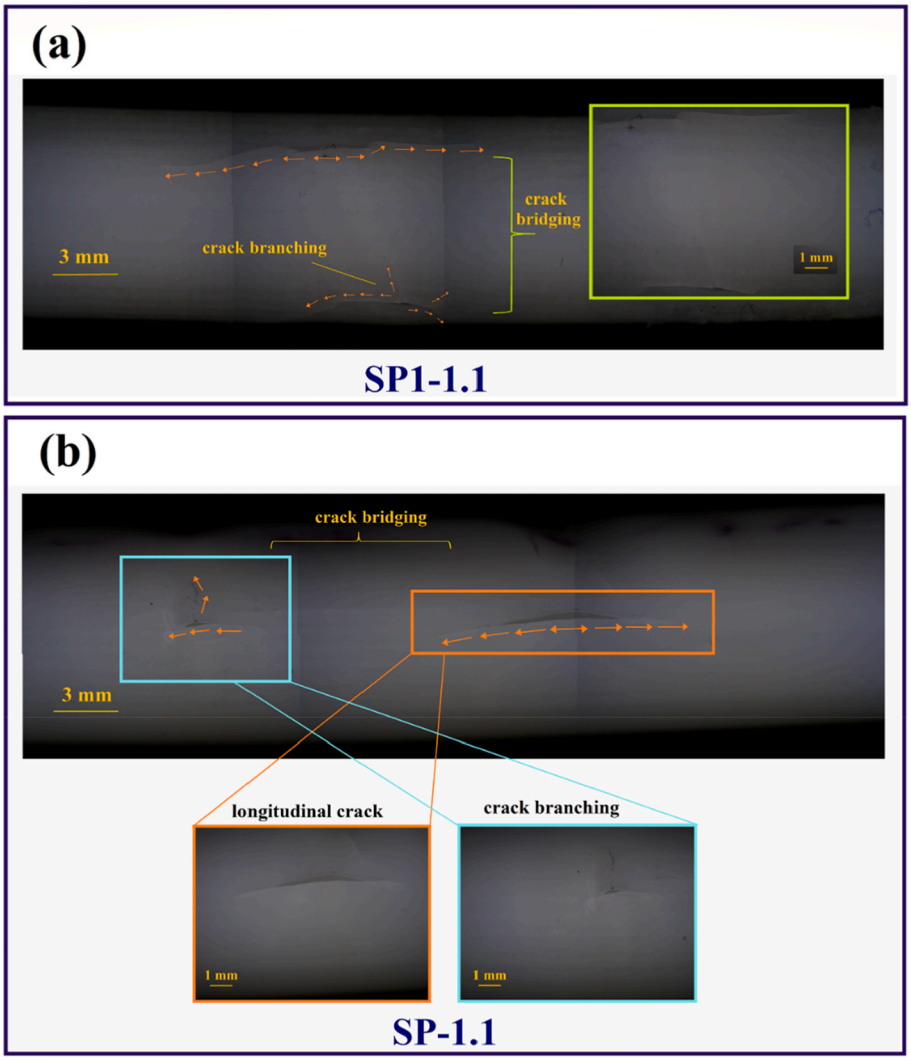

Fig. 8. Optical microscopy images of a) SP1-1.1 and b) SP-1.1.

absorb more energy and delay crack propagation further, adding an extra layer of toughness to the structure.

The ductile Titebond glue absorbs energy during deformation, which helps to delay crack initiation and propagation. This energy absorption leads to an improved toughness (Fig. 9e). Also, the ductile nature of the Titebond glue causes the cracks to deflect at the glue interface, creating a tortuous crack path (Fig. 9j). The change in the crack path is due to the higher energy required for the crack propagation which shows the effectiveness of this glue as an interlayer to improve the mechanical properties of the sample, thereby enhancing the fracture toughness. As a result, the redistribution of stress around the crack tip can reduce stress and delay catastrophic failure.

The brittle superglue absorbed little energy, leading to a more linear and less tortuous crack path (Fig. 9g–i). This resulted in a lower toughness compared to the ductile glue. The brittle glue interface does not significantly deflect cracks, leading to a more direct fracture path. The absence of crack deflection reduced the energy required for crack propagation.

4. Conclusion

This study is the first report on fabricating soft/hard laminated rods with architecture similar to spicules. The results showed that the ideal SISs with organic layers was SP1-1.1 (including Titbond adhesive in between the rigid cylinders) with flexural strength, strain, and modulus of 51.95 ± 6.53 MPa, 5.39 ± 1.11 %, and 0.66 ± 0.02 GPa, respectively. The results showed that the design of organic layers between the rigid cylinders resulted in higher flexibility and toughness than the SP-1.1. In the SP1-1.1 sample, a new crack-bridging mechanism was activated due to the presence of organic interlayers. The optical microscopy findings indicate that in SP1-1.1, the Titebond adhesive presence operates as a binding constraint, limiting the movement of adjacent rigid cylinders apart from each other and effectively absorbing the energy exerted by external forces. The crack branching, bridging, deflection as well as organic bridging were observed as toughening and strengthening mechanisms in both SIS samples with and without adhesive interlayers. Increasing the space between the layers above 1.1 mm decreased the strength of the sample.

CRediT authorship contribution statement

Sorour Sadeghzade: Writing – review & editing, Writing – original draft, Visualization, Validation, Software, Methodology, Investigation, Formal analysis, Data curation, Conceptualization. **Niloofar Fani:** Software, Formal analysis. **Ajinkya Nene:** Software, Investigation, Writing – review & editing. **Fariborz Tavangarian:** Writing – review & editing, Validation, Supervision, Project administration, Investigation, Funding acquisition, Formal analysis, Conceptualization.

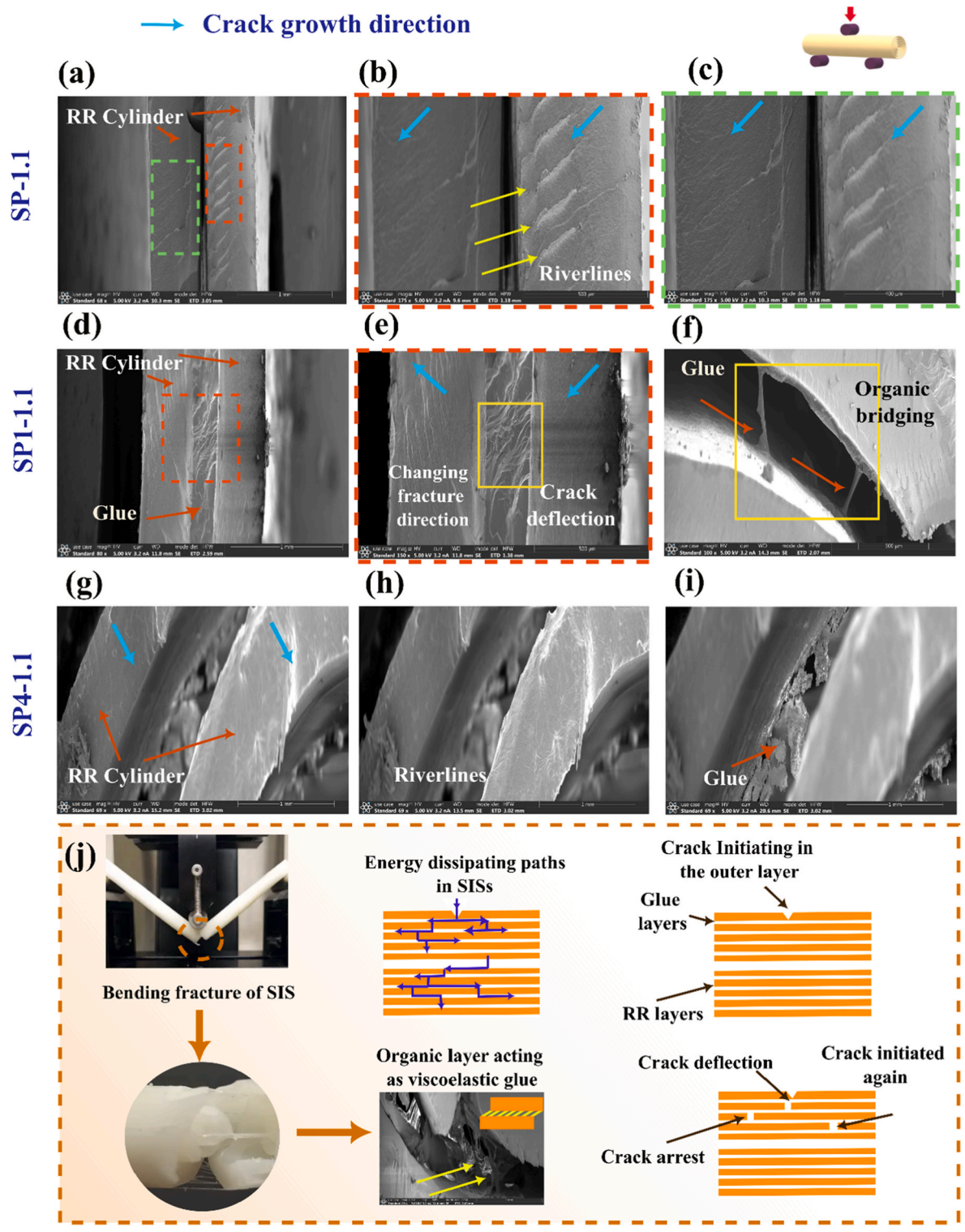

Fig. 9. SEM images of (a–c) SP-1.1, (d–f) SP1-1.1, (g–i) SP4-1.1 after bending test, (j) schematic representation of toughening mechanisms of spicule inspired structure composite samples and SP3-1.1 under bending test.

Declaration of competing interest

The authors declare that they have no known competing financial interests or personal relationships that could have appeared to influence the work reported in this paper.

Data availability

Data will be made available on request.

Acknowledgements

This project was partially supported by the NSF-CAREER under the NSF Cooperative Agreement CMMI-2146480, and by a seed grant from

Penn State Harrisburg's Office of Research and Outreach.

Appendix A. Supplementary data

Supplementary data to this article can be found online at https://doi.org/10.1016/j.compscitech.2024.110789.

References

[1] L. Zhu, R. Feng, X. Li, J. Xi, X. Wei, Design of lightweight tree-shaped internal support structures for 3D printed shell models, Rapid Prototyp. J. 25 (2019) 1552–1564, https://doi.org/10.1108/RPJ-04-2019-0108.

[2] O. Hussein, D.A. Geddes, S.A. Bernal, J.L. Provis, Lightweight foamed geopolymer. International Conference on Alkali Activated Materials and Geopolymers: Versatile Materials Offering High Performance and Low Emissions, 2018. https://dc.engconfintl.org/geopolymers/49.

[3] H.C. Schröder, V.A. Grebenjuk, X. Wang, W.E.G. Müller, Hierarchical architecture of sponge spicules: biocatalytic and structure-directing activity of silicatein proteins as model for bioinspired applications, Bioinspir. Biomim. 11 (2016) 041002, https://doi.org/10.1088/1748-3190/11/4/041002.

[4] P. Zhang, M.A. Heyne, A.C. To, Biomimetic staggered composites with highly enhanced energy dissipation: modeling, 3D printing, and testing, J. Mech. Phys. Solid. 83 (2015) 285–300.

[5] P. Fratzl, Biomimetic materials research: what can we really learn from nature's structural materials? J. R. Soc. Interface. 4 (2007) 637–642, https://doi.org/10.1098/rsif.2007.0218.

[6] F. Tavangarian, S. Sadeghzade, N. Fani, D. Khezrimotlagh, K. Davami, 3D-printed bioinspired spicules: strengthening and toughening via stereolithography, J. Mech. Behav. Biomed. Mater. 155 (2024) 106555, https://doi.org/10.1016/j.jmbbm.2024.106555.

[7] I. Sukia, A. Esnaola, B. Erice, J. Aurrekoetxea, Impact behaviour of bio-inspired sandwich panels integrally manufactured from 3D printed continuous carbon fibre reinforced polyamide, Compos. Sci. Technol. (2024) 110515.

[8] J. Sun, B. Bhushan, Hierarchical structure and mechanical properties of nacre: a review, RSC Adv. 2 (2012) 7617–7632, https://doi.org/10.1039/C2RA20218B.

[9] H. Bai, F. Walsh, B. Gludovatz, B. Delattre, C. Huang, Y. Chen, A.P. Tomsia, R. O. Ritchie, Bioinspired hydroxyapatite/poly(methyl methacrylate) composite with a nacre-mimetic architecture by a bidirectional freezing method, Adv. Mater. 28 (2016) 50–56, https://doi.org/10.1002/adma.201504313.

[10] A.Y.-M. Lin, M.A. Meyers, Interfacial shear strength in abalone nacre, J. Mech. Behav. Biomed. Mater. 2 (2009) 607–612, https://doi.org/10.1016/j.jmbbm.2009.04.003.

[11] (PDF) Biomimetic design of materials and biomaterials inspired by the structure of nacre, n.d. https://www.researchgate.net/publication/24269583_Biomimetic_design_of_materials_and_biomaterials_inspired_by_the_structure_of_nacre. (Accessed 13 June 2024).

[12] M. Rousseau, E. Lopez, P. Stempflé, M. Brendlé, L. Franke, A. Guette, R. Naslain, X. Bourrat, Multiscale structure of sheet nacre, Biomaterials 26 (2005) 6254–6262.

[13] I. Corni, T.J. Harvey, J.A. Wharton, K.R. Stokes, F.C. Walsh, R.J.K. Wood, A review of experimental techniques to produce a nacre-like structure, Bioinspiration Biomimetics 7 (2012) 031001, https://doi.org/10.1088/1748-3182/7/3/031001.

[14] Z. Wang, Y. Sun, H. Wu, C. Zhang, Low velocity impact resistance of bio-inspired building ceramic composites with nacre-like structure, Construct. Build. Mater. 169 (2018) 851–858.

[15] P. Fratzl, Biomimetic materials research: what can we really learn from nature's structural materials? J. R. Soc. Interface. 4 (2007) 637–642, https://doi.org/10.1098/rsif.2007.0218.

[16] V. Rodriguez-Garcia, M. Herráez, V. Martinez, R.G. de Villoria, Interlaminar and translaminar fracture toughness of Automated Manufactured Bio-inspired CFRP laminates, Compos. Sci. Technol. 219 (2022) 109236.

[17] Y. Chen, Z. Jin, W. Kang, Z. Liu, W. Yang, Y. Li, 3D printed bio-inspired self-similar carbon fiber reinforced composite sandwich structures for energy absorption, Compos. Sci. Technol. 248 (2024) 110453.

[18] X. Li, X. Zhang, Y. Yuan, Bio-inspired hybrid helicoidal microstructure: balancing carrying capacity and prolonged residual load, Compos. Sci. Technol. (2023) 110249.

[19] W.E. Müller, X. Wang, K. Kropf, H. Ushijima, W. Geurtsen, C. Eckert, M.N. Tahir, W. Tremel, A. Boreiko, U. Schloßmacher, Bioorganic/inorganic hybrid composition of sponge spicules: matrix of the giant spicules and of the comitalia of the deep sea hexactinellid Monorhaphis, J. Struct. Biol. 161 (2008) 188–203.

[20] G. Mayer, R. Trejo, E. Lara-Curzio, M. Rodriguez, K. Tran, H. Song, W.H. Ma, Lessons for New Classes of Inorganic/organic Composites from the Spicules and Skeleton of the Sea Sponge Euplectella Aspergillum, vol. 844, MRS Online Proceedings Library (OPL), 2004. Y4-2.

[21] S. Niu, B. Li, Z. Mu, M. Yang, J. Zhang, Z. Han, L. Ren, Excellent structure-based multifunction of morpho butterfly wings: a review, Journal of Bionic Engineering 12 (2015) 170–189.

[22] W.E.G. Müller, X. Wang, F.-Z. Cui, K.P. Jochum, W. Tremel, J. Bill, H.C. Schröder, F. Natalio, U. Schloßmacher, M. Wiens, Sponge spicules as blueprints for the biofabrication of inorganic–organic composites and biomaterials, Appl. Microbiol. Biotechnol. 83 (2009) 397–413, https://doi.org/10.1007/s00253-009-2014-8.

[23] J.C. Weaver, J. Aizenberg, G.E. Fantner, D. Kisailus, A. Woesz, P. Allen, K. Fields, M.J. Porter, F.W. Zok, P.K. Hansma, Hierarchical assembly of the siliceous skeletal lattice of the hexactinellid sponge Euplectella aspergillum, J. Struct. Biol. 158 (2007) 93–106.

[24] A. Woesz, J.C. Weaver, M. Kazanci, Y. Dauphin, J. Aizenberg, D.E. Morse, P. Fratzl, Micromechanical properties of biological silica in skeletons of deep-sea sponges, J. Mater. Res. 21 (2006) 2068–2078.

[25] V.C. Sundar, A.D. Yablon, J.L. Grazul, M. Ilan, J. Aizenberg, Fibre-optical features of a glass sponge, Nature 424 (2003) 899–900.

[26] J. Aizenberg, J.C. Weaver, M.S. Thanawala, V.C. Sundar, D.E. Morse, P. Fratzl, Skeleton of *Euplectella* sp.: structural hierarchy from the nanoscale to the macroscale, Science 309 (2005) 275–278, https://doi.org/10.1126/science.1112255.

[27] Z. Ding, H. Xiao, Y. Duan, B. Wang, Bio-inspired self-stitching for enhancing ductility and impact resistance of unidirectional laminated composites, Compos. Sci. Technol. 242 (2023) 110184, https://doi.org/10.1016/j.compscitech.2023.110184.

[28] M. Sarikaya, H. Fong, N. Sunderland, B.D. Flinn, G. Mayer, A. Mescher, E. Gaino, Biomimetic model of a sponge-spicular optical fiber—mechanical properties and structure, J. Mater. Res. 16 (2001) 1420–1428.

[29] H.C. Schröder, X. Wang, W. Tremel, H. Ushijima, W.E. Müller, Biofabrication of biosilica-glass by living organisms, Nat. Prod. Rep. 25 (2008) 455–474.

[30] M.A. Monn, J.C. Weaver, T. Zhang, J. Aizenberg, H. Kesari, New functional insights into the internal architecture of the laminated anchor spicules of *Euplectella aspergillum*, Proc. Natl. Acad. Sci. U.S.A. 112 (2015) 4976–4981, https://doi.org/10.1073/pnas.1415502112.

[31] G. Mayer, New toughening concepts for ceramic composites from rigid natural materials, J. Mech. Behav. Biomed. Mater. 4 (2011) 670–681.

[32] S. Sadeghzade, R. Emadi, M. Salehi, F. Tavangarian, A. Ramini, Crack propagation and toughening mechanisms of bio-inspired artificial spicules fabricated by additive manufacturing technique, Theor. Appl. Fract. Mech. 110 (2020) 102797.

[33] 1801088-TDS-ENUS-0.pdf, n.d. https://formlabs-media.formlabs.com/datasheets/1801088-TDS-ENUS-0.pdf. (Accessed 18 June 2024).

[34] G.D. Quinn, B.T. Sparenberg, P. Koshy, L.K. Ives, S. Jahanmir, D.D. Arola, Flexural strength of ceramic and glass rods, J. Test. Eval. 37 (2009) 222–244.

[35] J.M. Gere, B.J. Goodno, Mechanics of Materials, Cengage learning, 2012.

[36] G. Subhash, S. Ridgeway, Mechanics of Materials Laboratory Course, Springer Nature, 2022.

[37] Y. Yang, X. Li, M. Chu, H. Sun, J. Jin, K. Yu, Q. Wang, Q. Zhou, Y. Chen, Electrically assisted 3D printing of nacre-inspired structures with self-sensing capability, Sci. Adv. 5 (2019) eaau9490, https://doi.org/10.1126/sciadv.aau9490.

[38] S. Sadeghzade, R. Emadi, S. Labbaf, Formation mechanism of nano-hardystonite powder prepared by mechanochemical synthesis, Adv. Powder Technol. 27 (2016) 2238–2244.

[39] S. Sadeghzade, R. Emadi, F. Tavangarian, Combustion assisted synthesis of hardystonite nanopowder, Ceram. Int. 42 (2016) 14656–14660.

[40] S. Sadeghzade, R. Emadi, H. Ghomi, Mechanical alloying synthesis of forsterite-diopside nanocomposite powder for using in tissue engineering, Ceramics 59 (2015) 1–5.

[41] S. Ghorbanzadeh Sheish, R. Emadi, M. Ahmadian, S. Sadeghzade, F. Tavangarian, Fabrication and characterization of polyvinylpyrrolidone-eggshell membrane-reduced graphene oxide nanofibers for tissue engineering applications, Polymers 13 (2021) 913.

[42] S. Sadeghzade, J. Cao, D. Zhang, P. Dong, J. Hu, A. Es' haghioskui, H. Yuan, Soft acrylate monomer-based optically clear adhesive for foldable electronics: mechanical characterization and fractography analysis under large strain, Eur. Polym. J. 197 (2023) 112337.

[43] S. Sadeghzade, R. Emadi, T. Ahmadi, F. Tavangarian, Synthesis, characterization and strengthening mechanism of modified and unmodified porous diopside/baghdadite scaffolds, Mater. Chem. Phys. 228 (2019) 89–97.

[44] X. Song, Slurry Based Stereolithography: a Solid Freeform Fabrication Method of Ceramics and Composites, University of Southern California, 2016. PhD Thesis.

[45] S. Sadeghzade, R. Emadi, F. Tavangarian, A. Doostmohammadi, In vitro evaluation of diopside/baghdadite bioceramic scaffolds modified by polycaprolactone fumarate polymer coating, Mater. Sci. Eng. C 106 (2020) 110176.

[46] S. Morankar, A. Kumar, A. Luktuke, N. Chawla, Influence of hydration on the micromechanical properties of silica spicules from the Venus flower basket (Euplectella aspergillum), JOM 75 (2023) 3816–3826.

[47] F. Tavangarian, S. Sadeghzade, K. Davami, A novel biomimetic design inspired by nested cylindrical structures of spicules, J. Alloys Compd. 864 (2021) 158197.